On the practical limitations for the generation of Gunn oscillations in highly doped GaN diodes

S. García-Sánchez[1], M. Abou Daher[2], M. Lesecq[2], L. Huo[3], R. Lingaparthi[3], D. Nethaji[3], K. Radhakrishnan[3], I. Íñiguez-de-la-Torre[1], B. G. Vasallo[1], S. Pérez[1], T. González[1], Senior Member, IEEE, and J. Mateos[1], Member, IEEE

Abstract— Planar Gunn diodes based on doped GaN active layers with different geometries have been fabricated and characterized. Gunn oscillations have not been observed due to the catastrophic breakdown of the diodes for applied voltages around 20-25 V, much below the bias theoretically needed for the onset of Gunn oscillations. The breakdown of the diodes has been analyzed by pulsed *I-V* measurements at low temperature, and it has been observed to be almost independent of the geometry of the channels, thus allowing to discard self-heating effects as the origin of the device burning. The other possible mechanism for the device failure is impact-ionization avalanche due to the high electric fields present at the anode corner of the isolating trenches. However, Monte Carlo simulations using the typical value of the intervalley energy separation of GaN, $\boldsymbol{\varepsilon_{1-2}}$ =2.2 eV, show that impact ionization mechanisms are not significant for the voltages for which the experimental failure is observed. But recent experiments showed that $\boldsymbol{\varepsilon_{1-2}}$ is lower, around 0.9 eV. This lower intervalley separation leads to a much lower threshold voltage for the Gunn oscillations, not far from the experimental breakdown. Therefore, we attribute the devices failure to an avalanche process just when Gunn domains start to form, since they increase the population of electrons at the high electric field region, thus strongly enhancing impact ionization mechanisms which lead to the diode failure.

Index Terms— Gunn diodes, doped GaN, THz generation, Monte Carlo simulations

I. Introduction

The sub-THz and THz ranges of frequency (above 100 GHz, approximately) are of great interest for a wide variety of applications, since such electromagnetic radiation is non-ionising (safe to use on humans) and can penetrate many visually opaque materials, thus being potentially useful in diverse fields such as medical imaging or security scanning [1]-[4]. THz frequencies also have interesting spectroscopic capabilities for pharmaceutical industry, thus allowing the possibility of fabrication of sensors of explosives or biological agents such as anthrax. High speed data transfer using high frequency sub-THz carriers also opens the possibility of ultra-high data rate transfer [5]. However, the lack of powerful continuous-wave, compact, tunable room temperature (and hopefully cheap) THz sources has delayed the widespread use of such applications. Apart from quantum cascade lasers (which must be operated at cryogenic temperatures) [6], in the last years, strong advances have been made with resonant tunneling diode technology [7], which has allowed to demonstrate THz generation with output power in the μW range using single devices up to ∼2 THz [8]-[10] and reaching 0.73 mW for an 89-element array at ∼1 THz [11]. However, up to now, the state-of-the-art output power levels (near 1 mW of power at 1.6 THz and 50 μW at 2.5 THz) have been obtained with classic frequency multiplied sources based on GaAs Schottky diodes [12]-[17], which are also presently taking advantage of the increased input power levels provided by power amplifiers around and above 100 GHz. In any case, although a huge research work is being made both from electronic and optic approaches to explore the so-called THz gap, there is still much road to travel in order to make consumer applications broadly accessible. That is why novel technologies based on wide bandgap semiconductors such as Gallium Nitride (GaN) are emerging as highly promising materials for high power applications in the millimeter wavelengths [18]-[21]. The development of GaN technology is already providing significant advances on the efficiency of practical power electronics systems at the microwave frequency range, but it also appears as a candidate for power generation at sub-THz frequencies by means of active two-terminal devices like Gunn diodes [22], which generate output power based on the presence of a negative differential resistance (NDR). Although there has not been yet a demonstration of an operational GaN-based Gunn diode, simulations [23]-[28] and indirect evidences of current oscillations in GaN structures [29]-[31] allow us to believe in the practical feasibility of high-power high-frequency GaN Gunn diodes.

Instead of the Gunn diode design based on a vertical geometry of Refs. [29]-[31], we have chosen a planar (horizontal) approach. Inspired on the self-switching diode concept [32], Planar Gunn Diodes (PGDs) with shaped nanochannels were proposed to improve the efficiency of Gunn oscillations exploiting the flexibility of their design [33]. Initially, AlGaN/GaN epilayers were used to fabricate these PGDs, but in spite of the optimization of their design using

Manuscript received ¿? 2022; revised ¿? 2022; accepted ¿? 2022. Date of publication ¿? 2022; date of current version ¿? 2022.This work has been partially supported through grant PID2020-115842RB-I00 funded by MCIN/AEI/10.13039/501100011033.

S. García-Sánchez, I. Íñiguez de la Torre, B. G. Vasallo, S. Pérez, T. González and J. Mateos, are with the Applied Physics Department, and USAL-NANOLAB, Universidad de Salamanca, Salamanca, Spain.

M. Abou Daher and M. Lesecq are with IEMN - Institut d'Electronique de Microélectronique et de Nanotechnologie, Lille, France.

L. Huo, R. Lingaparthi, D. Nethaji and K. Radhakrishnan are with UMI3288 CINTRA, (CNRS/NTU/THALES), Nanyang Technological University, Singapore.

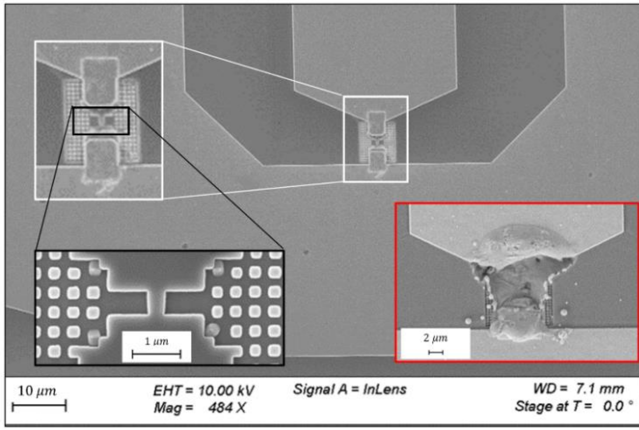

Fig. 1. SEM picture of a fabricated diode formed of a tapered channel with W_i=300 nm, W_o=350 nm and L=0.5 µm. The bottom right picture shows a diode after its catastrophic failure, where anode and cathode are short-circuited by the melted metallic pads.

tapered channels [34], no evidence of Gunn oscillations has been found yet (in different runs of fabricated diodes), even when applying voltages in excess of 40 V, above the theoretical threshold for the onset of the oscillations. Monte Carlo (MC) simulations show that by using highly doped GaN as the active layer, Gunn oscillations can be more effectively obtained [35]. The first shaped nanochannels based on doped GaN active layers have been manufactured [35]-[37], unfortunately showing a premature breakdown at low voltages, not linked to thermal dissipation.

The aim of this work is to use the MC method to check, first, the validity of the previously published simulations of Gunn oscillations in light of measurements [38], [39] that indicate that the energy separation between the Γ_1-valley of GaN (the minimum of the conduction band) and the first satellite valley is around 0.9 eV, lower than the value typically used in the published simulations, 2.2 eV [23]-[28] or 1.9 eV [40], [41]. And, second, identify the origin of the breakdown of fabricated devices, for which a failure mechanism not linked to thermal heating is leading to the catastrophic damage of the devices for voltages much lower than expected. For this sake, both single particle MC simulations and a 2D ensemble MC self-consistently coupled with the solution of the Poisson equation, in which the ionization mechanism is included, will be used.

The paper is organized as follows. In Section II, we describe the fabrication of the devices and present the results of their characterization. In Section III the MC model and the simulations of bulk GaN are presented, and, in Section IV, we show the results of 2D MC simulations of Gunn diodes. Finally, the main conclusions of our work are drawn in Section V.

II. Experimental Results

The devices were fabricated on a GaN epilayer grown on double side polished semi-insulating 4H-SiC (001) substrate using plasma assisted molecular beam epitaxy. A 150 nm thick active layer of highly doped (nominally N_D=10^{19}cm^{-3}) GaN was grown on the top of an undoped GaN buffer and a AlN nucleation layer using the process described in Refs. [35], [37], [42]. The thickness and doping level of the active layer were

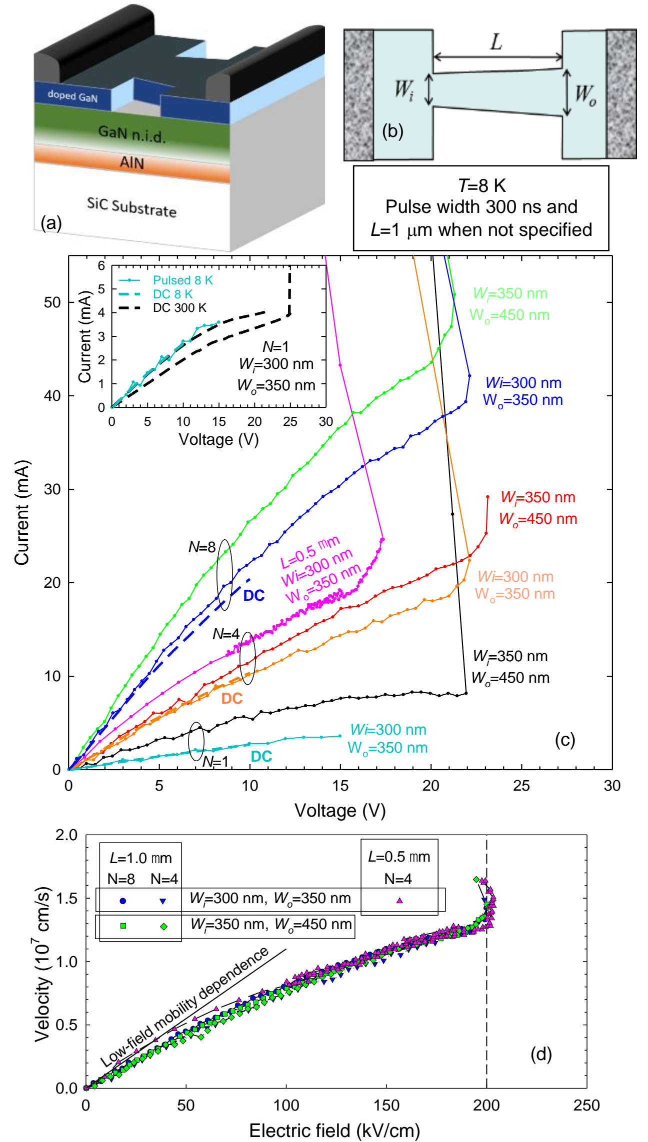

Fig. 2. (a) 3D and (b) top-view sketch of a single channel device. (c) Pulsed measurements performed at T=8 K using 300 ns-width pulses (1% duty cycle) in order to avoid as much as possible self-heating effects (thin solid lines with dots). Results are shown for arrays of N=1, 4 and 8 diodes with L=1 µm and two different channel width configurations: (i) W_i=300 nm and W_o=350 nm and (ii) W_i=350 nm and W_o=450 nm. In order to demonstrate that self-heating effects are almost negligible, the DC measurements for the diodes with W_i=300 nm and W_o=350 nm are also plotted with thick dashed lines. The result for an array of 4 channels with a shorter length L=0.5 µm and W_i=300 nm and W_o=350 nm is also shown for comparison. The inset shows the I-V curves obtained with DC measurements at T=8 and 300 K (providing similar values, as expected from the nearly temperature-independent values of mobility and sheet electron density) for a single channel diode (N=1) with L=1 µm, W_i=300 nm and W_o=350 nm compared with the pulsed results at T=8 K. Two consecutive sweeps at 300 K applying voltages up to 22 and 25 V, respectively, are represented (failure was observed in the second sweep). (d) Velocity-field dependence extracted from the pulsed measurements of devices with different geometries shown in (c). The linear dependence given by the low-field mobility (110 cm^{2}/V·s at 8 K) is also plotted.

optimized by means of MC simulations [28] to enhance the Gunn oscillations, trying to avoid as much as possible self-heating effects. Hall measurements show that the electron density is slightly lower than expected n=6.0×10^{18}cm^{-3} (and almost constant in the 8-300 K temperature range) with a mobility of 170 cm^{-2}/V·s at room temperature (decreasing to around 110 cm^{-2}/V·s at 8 K).

Diodes made of arrays of parallel tapered channels with different geometries were fabricated by electron beam lithography and $Ar/Cl_2/BCl_3$ plasma etching. Fig. 1 shows the example of a single tapered channel with input width W_i=300 nm, output width W_o=350 nm and length L=1 µm, whose 3D and top-view shape is shown in Fig. 2(a) and (b).

Low temperature experiments were performed using a Lakeshore cryogenic probe station to avoid as much as possible the heating of the diodes, trying to overcome the catastrophic breakdown due to thermal effects often experienced at room temperature in this type of devices [31]. Pulsed measurements were obtained with a 4225-PMU Ultra Fast I-V module of a Keithley 4200-SCS semiconductor parameter analyzer. 300 ns pulses with 1% duty cycle were used to avoid the self-heating of the devices. Due to the low current level provided by the nanochannels, a current decrease between DC and pulsed measurements is only observed for N=8, when the dissipated power is above ~0.1-0.2 W. As clearly observed in Fig. 2, low-temperature pulsed bias conditions are not able to avoid the failure of the devices at voltages below 25 V. Indeed, the breakdown voltage is similar to that obtained under DC bias conditions and at room temperature for N=1 (see inset), as expected due to the negligible self-heating effects.

Fig. 2(d) shows the electron velocity vs. electric field (v-E) characteristic extracted from the pulsed I-V measurements of Fig. 2(c). The calculation has been made using W_i as the width of the channel (the limiting geometrical factor) and considering 10 nm of surface depletion at each side and at the top of the channel, a relatively low value due to the high doping level of the active layer. This value has been obtained by means of MC simulations. In order to estimate the value of the electric field, the voltage drop within the channel has been calculated by considering access resistances with values between 25 and 300 Ω (depending on the geometry), in good agreement with the experimental sheet and contact resistances. Even if the non-rectangular shape of the channel leads to a non-homogeneous distribution of the electric field and to lower-than-expected values of the electron velocity at high fields, the low-field mobility is well reproduced. But the most interestingly fact is that the device failure takes place when the electric field within the channel reaches about 200 kV/cm (for devices with both L=1.0 and 0.5 µm), just the value for which the peak velocity is found and the onset of NDR takes place.

The failure of the devices in absence of self-heating effects, together with the fact that the breakdown electric field is nearly independent of the geometry of the devices and the number of parallel channels, are strong indications of a non-thermal origin of the device burning. This is confirmed by the thermal measurements made at 70ºC under continuous DC bias, Fig. 3, showing that the temperature reached by the diodes strongly depends on the number of channels of the array, with the single-channel devices showing a temperature increase due to self-heating effects of just around 40 degrees when applying a DC bias of 12 V (corresponding to a power of about 60 mW), one third of what is observed for N=8 at the same bias (with much larger P_{DC}=380 mW). As a consequence, we attribute the failure of the devices to a mechanism related to the high electric fields appearing within the channels. This assumption is

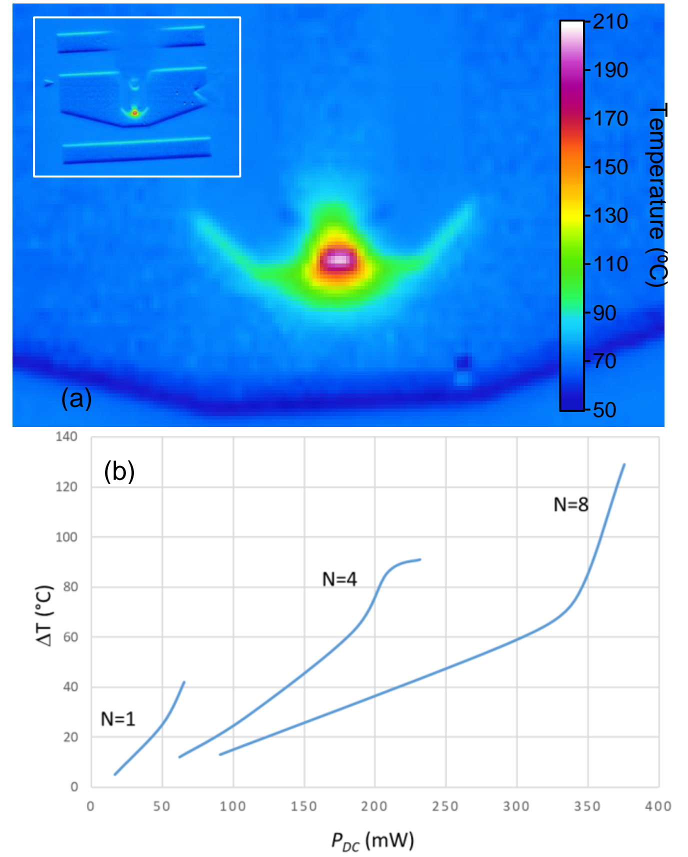

Fig. 3. (a) Picture taken with a high-definition thermographic infrared camera of an array of 8 diodes with W_i=350 nm, W_o=550 nm and L=1 µm when applying a DC bias of 11 V (with a dissipated power of about P_{DC}=380 mW) with the samples heated at 70ºC to be in the optimum range of precision of the camera. (b) Maximum of the recorded temperature increase vs. applied DC power for arrays with N=1, 4 and 8 channels. The maximum temperature at the hottest point could be slightly higher because the pixel size of the camera is 3 µm×3 µm, larger than the size of the channels, so that some temperature averaging is unavoidable.

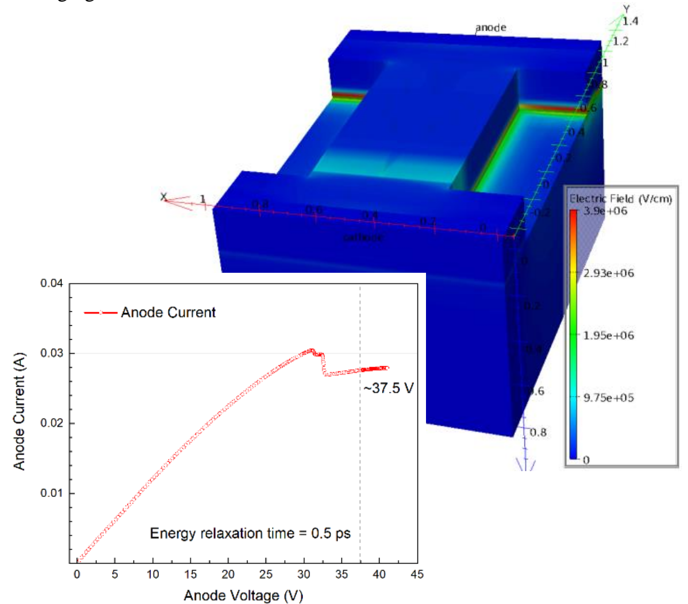

Fig. 4. I-V curve and 3D map of the electric field of a GaN rectangular channel 500 nm wide and 1.0 µm long, doped at N_D=2×10^{18} cm^{-3}, for an applied bias of V=37 V (above the onset of Gunn oscillations). Results obtained with the commercial TCAD Silvaco ATLAS simulator using the Energy Balance model.

supported by the fact that the breakdown electric field is independent of the channel geometry and coincides with the onset of the NDR, see Fig. 2(d), regardless of the current level.

The 3D simulations (using Silvaco ATLAS) presented in Fig. 4 evidence the presence of Gunn oscillations, but more importantly, show the location of an electric field hot-spot (with values well above the MV/cm range) at the bottom corner of the trenches in the anode side. This kind of simulations, even if they are able to reproduce the main features of the electrical characteristics of Gunn diodes, and can provide valuable information about the electric field distribution, are not the most adequate tool to study the influence of the material parameters, such as the intervalley separation, on the performance of the devices. That is why in the next section we introduce the detailed modelling of the diodes by means of MC simulations.

III. Monte Carlo Simulations of Bulk GaN

With the aim of analyzing the microscopic transport processes of electrons in GaN, first, a single-particle Monte Carlo (MC) simulator has been employed. The scattering mechanisms included in the simulations are intervalley, acoustic and optical (polar and non-polar) phonons, piezoelectric and ionized impurities. The conduction band of GaN has been modelled by a three non-parabolic, spherical valley model (Γ_1, U and Γ_3 valleys) by considering the Wurzite structure, the stable phase of GaN at ambient pressure. The parameters used in the MC model of GaN were presented in Ref. [25]. Impact ionization phenomena have been included in our MC model as an additional scattering mechanism by using the Keldysh approach [40], [41], [43]-[45], where the probability per unit time of having an impact ionization event, $\boldsymbol{P(\varepsilon)}$, is given by:

$$\boldsymbol{P(\varepsilon)} = \begin{cases} \boldsymbol{S\cdot\left(\frac{\varepsilon-\varepsilon_{th}}{\varepsilon_{th}}\right)^{k}} \textbf{ if } \boldsymbol{\varepsilon > \varepsilon_{th}} \\ \textbf{0 if } \boldsymbol{\varepsilon \le \varepsilon_{th}} \end{cases} \qquad (1)$$

where $\boldsymbol{\varepsilon}$ is the total electron energy (calculated as the addition of kinetic energy plus intervalley separation), $\boldsymbol{\varepsilon_{th}}$ is the threshold energy for impact ionization, and $\boldsymbol{S}$ and $\boldsymbol{k}$ are parameters which allow to tune the softness or hardness of the ionization threshold.

The lowest point of the conduction band is located at the Γ point (Γ_1-valley), 3.44 eV above the absolute maximum of the valence band, also located at the Γ point. The second minimum is located between the *M* and *L* points, leading to a valley called the *U*-valley. The energy separation between the first and the second valley is typically considered to be around 2.0 eV ($\boldsymbol{\varepsilon_{1-2}}$ =2.2 eV in [23]-[28] and 1.9 eV [40], [41]), but recent experiments have revealed a much lower value of 0.9 eV [38], [39], not yet contemplated in the literature of MC simulations of GaN. Both values will be considered in our simulations to explore the implications both on the generation of Gunn oscillations and on the possible breakdown mechanisms.

In spite of the large effort and meticulous techniques used to precisely measure the impact ionization coefficients in GaN [46]-[48], experimental data exhibit a substantial dispersion. Moreover, due to the anisotropy of GaN, the experimental results obtained in vertical diodes are not easy to adjust with our model (the value of *k* should be hugely increased). That is why we have taken the results obtained with *ab-initio* simulations

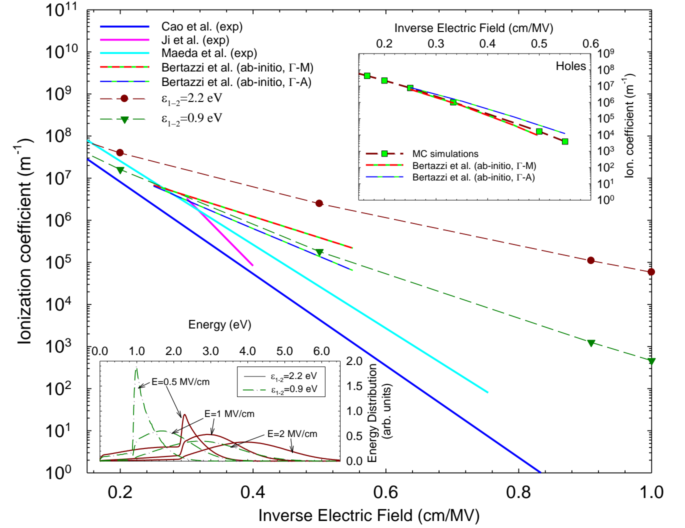

Fig. 5. Ionization coefficients vs. inverse electric field obtained with MC simulations using $\boldsymbol{\varepsilon_{th}}$=3.5 eV, *k*=4, and *S*=$10^{13}$ s^{-1}, for intervalley energy separations of $\boldsymbol{\varepsilon_{1-2}}$=2.2 and 0.9 eV. The insets show the impact ionization coefficient for holes and the distribution function of the total energy for electric fields of 0.5, 1.0 and 2.0 MV/cm.

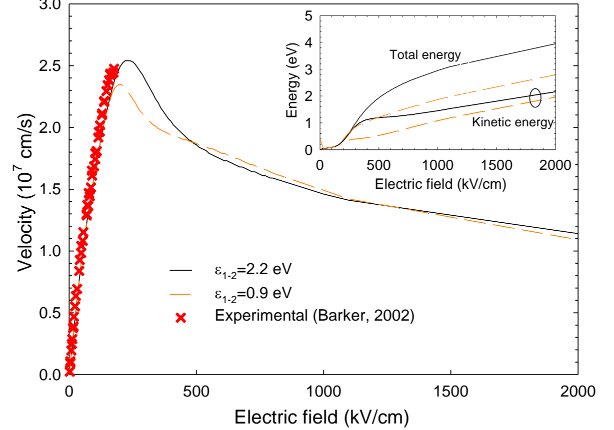

Fig. 6. Average velocity of electrons vs. electric field, *E*, for GaN doped at N_D=5×10^{18} cm^{-3} at room temperature for $\boldsymbol{\varepsilon_{1-2}}$=2.2 and 0.9 eV compared with the experimental measurements of [51]. The inset shows the average total and kinetic energies vs. *E*.

using the pseudo-potential method [43] as reference to adjust the parameters of the Keldysh formula ($\boldsymbol{\varepsilon_{th}}$, *S* and *k*). Fig. 5 evidences a good agreement of the results obtained with our isotropic MC transport model (mainly when using $\boldsymbol{\varepsilon_{1-2}}$=0.9 eV) with the results of [43], falling between the results for the Γ-M and Γ-A directions by considering $\boldsymbol{\varepsilon_{th}}$=3.5 eV, *S*=$10^{13}$ s^{-1} and *k*=4 (well within the range of values found in literature [40], [41]). As expected, the impact ionization coefficient of electrons is smaller for $\boldsymbol{\varepsilon_{1-2}}$=0.9 eV than for 2.2 eV, and the dependence with 1/*E* steeper due to a completely different electron energy distribution, see the inset of Fig. 5; electrons reach much lower energies when reducing the value of $\boldsymbol{\varepsilon_{1-2}}$. The values of the impact ionization coefficient for holes, see inset of Fig. 5, show also a good agreement with the results of [43], but they are not significant for the study made in this work since we are interested in the process that gives rise to the avalanche mechanism, which are the impact ionization events originated by hot electrons leaked through the GaN buffer, and we do not observe a significant

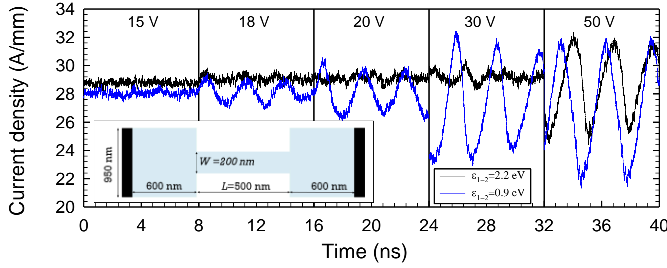

Fig. 7. Time-sequences of current density for a 200 nm wide 0.5 μm long GaN channel (geometry shown in the inset), doped at N_D=5×10^{18} cm^{-3}, for applied biases of V=15, 18, 20, 30 and 50 V, considering $\boldsymbol{\varepsilon_{1-2}}$=2.2 and 0.9 eV. The inset shows the geometry of the top-view simulations of the n-doped GaN channel.

number of secondary ionizations initiated by the generated holes for the bias conditions considered here.

The influence of the intervalley separation on the v-E curve can be observed in Fig. 6 (considering N_D=5×10^{18} cm^{-3}). When decreasing $\boldsymbol{\varepsilon_{1-2}}$ from 2.2 to 0.9 eV both the peak velocity and the critical electric field are slightly decreased (from 2,54 to 2.35×10^7 cm/s and from 220 to 180 kV/cm, respectively). This happens due to the onset of intervalley scattering at lower electronic energies. The agreement of both curves with the experimental measurements of [51] is similar, since they are only possible below 200 kV/cm. As shown in the inset of Fig. 6, the average total and kinetic energies of electrons are much lower for $\boldsymbol{\varepsilon_{1-2}}$=0.9 eV once the population of the U-valley starts to be significant (for E above 320 kV/cm, approximately). From the point of view of the fabrication of Gunn diodes, this would be beneficial for lowering the threshold voltage for the onset of the current oscillations (and also for somewhat suppressing impact ionization mechanisms), as we will see in the next section.

IV. 2D Monte Carlo Simulations

In a previous work, we showed how 2D MC simulations of doped GaN channels exhibit Gunn oscillations, whose amplitude and frequency depend on the active layer thickness and doping level [28]. In that work, a value of $\boldsymbol{\varepsilon_{1-2}}$ =2.2 eV was used. The effect of the reduction $\boldsymbol{\varepsilon_{1-2}}$ on the characteristics of the Gunn oscillations is shown in Fig. 7 for a rectangular channel with L=0.5 μm, W=200 nm and N_D=5×10^{18} cm^{-3}, using a self-consistent surface-charge model (more details can be found in [49]). The figure presents time sequences of current density for different applied voltages (between 15 and 50 V) obtained with top-view simulations [34], i.e., considering a thick enough active layer. It is found that the threshold voltage for the onset of Gunn oscillations significantly decreases from around 45 V to about 18 V when $\boldsymbol{\varepsilon_{1-2}}$ is lowered from 2.2 to 0.9 eV. This is due to the modification of the v-E dependence shown in Fig. 6, where the negative differential mobility starts for a lower electric field (180 kV/cm instead of 220 kV/cm).

These effects are observed independently of the geometry of the diode studied, since they are related to the v-E characteristics of the material. Therefore, if the correct value for $\boldsymbol{\varepsilon_{1-2}}$ is confirmed to be as low as 0.9 eV, Gunn oscillations would be much easier to obtain than expected, since the voltages to be applied and, as a consequence, the DC power, would be much lower (less than 50%). This would relax the heat

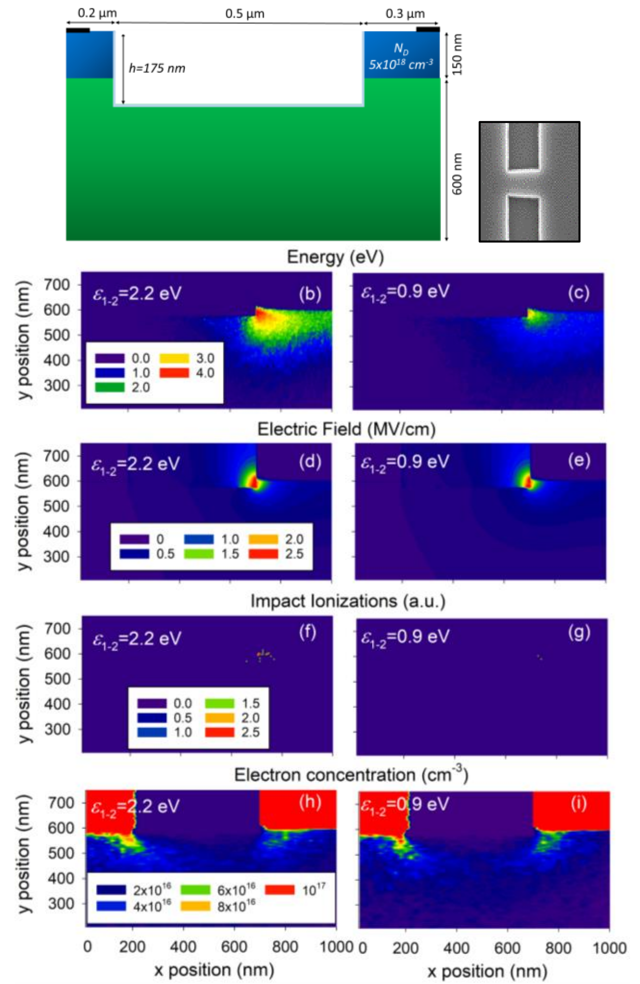

Fig. 8. Color maps of the significant internal quantities obtained with the MC simulations of the structure with the geometry depicted in (a) at room temperature for an applied bias of 20 V: (b) and (c) total energy, (d) and (e) electric field, (f) and (g) number of impact ionizations and (h) and (i) electron concentration (only the low concentration range is represented in order to well evidence the electrons flowing below the isolation). Results are shown for both $\boldsymbol{\varepsilon_{1-2}}$=2.2 eV in (b), (d), (f) and (h) and 0.9 eV in (c), (e), (g) and (i).

dissipation requirements, which is one of the main constraints for the practical implementation of GaN Gunn diodes. In any case, in the experimental characterization of the fabricated diodes presented in Section II, the devices are burnt before Gunn oscillations are observed. However, significantly, the breakdown voltage is not far from what is expected to be the threshold for the onset of the Gunn oscillations if one considers $\boldsymbol{\varepsilon_{1-2}}$=0.9 eV.

In order to investigate the origin of the catastrophic breakdown observed in the experiments, we have carried out 2D MC simulations of the high field region observed in the 3D simulations of Fig. 4. For that sake, the structure with the geometry shown in Fig. 8(a), representing a longitudinal cut at the etched sides of a channel of L=0.5 μm with an isolation depth of h=175 nm (we have used air as dielectric, as in the fabricated devices), has been simulated. Figs. 8(b) and (c) show that, for an applied bias of 20 V, the energy of electrons at the right corner of the isolation trench (where the electric field is maximum, on the MV/cm range) reaches very high values, above 3 eV, thus allowing for the onset of impact ionization processes, Figs. 8(f) and (g). However, they are not very

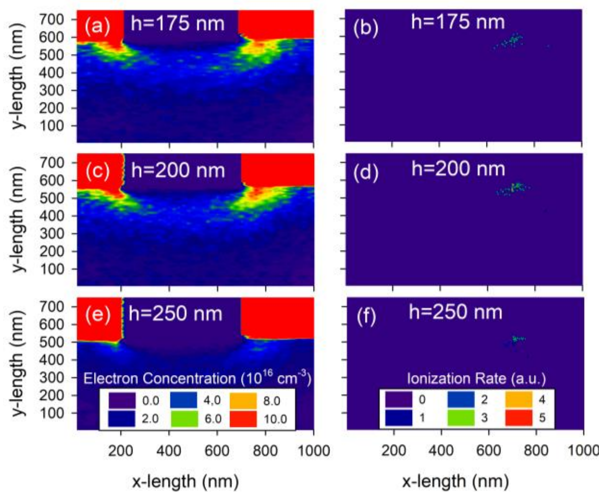

Fig. 9. Maps of (a), (c), and (e) electron concentration and (b), (d), (f) impact ionization events for *V*=30 V and different depths of the isolation trenches: (a) and (b) 175 nm, (c) and (d) 200 nm and (e) and (f) 250 nm.

frequent because the electron concentration at that point is quite low, only electrons reaching the anode by passing below the isolation trench populate that region [see Figs. 8(h) and (i)]. As a consequence, this cannot be the sole cause of the breakdown observed experimentally. Anyhow, we still attribute the failure of the devices to the onset of impact ionization processes, since they will be boosted when Gunn domains start to be formed. At that point the avalanche is provoked because (i) the electric field will be enhanced at the anode side of the channel and the surrounding regions, together with the fact (ii) that electrons in the high field domains will be able to leave the channel and go below the dielectric, thus reaching more easily the high field region at the anode corner of the isolation trench.

Lowering $\boldsymbol{\varepsilon_{1-2}}$ from 2.2 to 0.9 eV reduces the amount of impact ionization processes, but even if the average energy of electrons is reduced, still some impact ionization mechanisms appear. The results shown in Fig. 9 indicate that improving the isolation by realizing deeper trenches (or adding an ion implantation step as in [50]) could be the way to reduce the effect of impact ionization processes and thus avoid the failure of the diodes. A value of the depth of the trenches around 250 nm (100 nm deeper than the active layer thickness) would be enough to almost completely avoid the leakage current and thus protect the diodes from failure.

V. Conclusions

Using a doped GaN active layer, planar Gunn diodes have been fabricated and characterized. Low temperature pulsed *I-V* characterization of diodes with different geometries have allowed us to discard self-heating as the origin of the breakdown observed when biasing the devices. Device burning takes place at voltages for which Gunn oscillations are not yet expected by simulations made using the standard value of the intervalley separation $\boldsymbol{\varepsilon_{1-2}}$=2.2 eV. The results of our experiments and simulations indicate that the value of $\boldsymbol{\varepsilon_{1-2}}$ may be lower, 0.9 eV, than that typically used in the published simulations, as indicated by recent experiments [38], [39]. This value of $\boldsymbol{\varepsilon_{1-2}}$ allows to explain the catastrophic breakdown of the Gunn diodes, since the threshold voltage for the onset of the oscillations is much lower than that predicted by the standard GaN models. We attribute the device failure at applied voltages just at the onset of Gunn oscillations to an avalanche process started by the formation of Gunn domains, which strongly enhance the impact ionization processes at the electric field hot-spot located at the anode corner of the isolation trenches.

References

[1] R. Appleby and H. B. Wallace, "Standoff Detection of Weapons and Contraband in the 100 GHz to 1 THz Region," *IEEE Transactions on Antennas and Propagation,* vol. 55, *(11),* pp. 2944-2956, 2007. . DOI: 10.1109/TAP.2007.908543.

[2] C. Yu *et al*, "The potential of terahertz imaging for cancer diagnosis: A review of investigations to date," *Quantitative Imaging in Medicine and Surgery,* vol. 2, *(1),* pp. 33, 2012.

[3] D. Arnone, C. Ciesla and M. Pepper, "Terahertz imaging comes into view," *Physics World,* vol. 4, pp. 35-40, 2000.

[4] D. D. Arnone *et al*, "Applications of terahertz (THz) technology to medical imaging," in *Industrial Lasers and Inspection (EUROPTO Series),* 1999, pp. 209-219.

[5] M. J. Fitch and R. Osiander, "Terahertz waves for communications and sensing," *Johns Hopkins APL Tech. Dig.,* vol. 25, *(4),* pp. 348-355, 2004.

[6] M. A. Belkin *et al*, "Terahertz quantum-cascade-laser source based on intracavity difference-frequency generation," *Nature Photonics,* vol. 1, *(5),* pp. 288-292, 2007.

[7] M. Asada and S. Suzuki, "THz resonant tunneling devices," in *Fundamentals of Terahertz Devices and Applications* John Wiley & Sons Ltd., 2021, pp. 447-477.

[8] T. Maekawa *et al*, "Frequency increase in terahertz oscillation of resonant tunnelling diode up to 1.55 THz by reduced slot-antenna length," *Electron. Lett.,* vol. 50, *(17),* pp. 1214-1216, 2014. Available: https://doi.org/10.1049/el.2014.2362. DOI: 10.1049/el.2014.2362.

[9] S. Suzuki *et al*, "Fundamental oscillation of resonant tunneling diodes above 1 THz at room temperature," *Appl. Phys. Lett.,* vol. 97, *(24),* pp. 242102, 2010. Available: https://doi.org/10.1063/1.3525834. DOI: 10.1063/1.3525834.

[10] T. Maekawa *et al*, "Oscillation up to 1.92 THz in resonant tunneling diode by reduced conduction loss," *Applied Physics Express,* vol. 9, *(2),* pp. 024101, 2016. Available: https://dx.doi.org/10.7567/APEX.9.024101. DOI: 10.7567/APEX.9.024101.

[11] K. Kasagi, S. Suzuki and M. Asada, "Large-scale array of resonant-tunneling-diode terahertz oscillators for high output power at 1 THz," *J. Appl. Phys.,* vol. 125, *(15),* pp. 151601, 2019. Available: https://doi.org/10.1063/1.5051007. DOI: 10.1063/1.5051007.

[12] A. Maestrini *et al*, "A frequency-multiplied source with more than 1 mW of power across the 840–900-GHz band," *Microwave Theory and Techniques, IEEE Transactions On,* vol. 58, *(7),* pp. 1925-1932, 2010.

[13] J. V. Siles and J. Grajal, "Capabilities of GaN schottky multipliers for LO power generation at millimeter-wave bands," in *Proc. 19th International Symposium on Space Terahertz Technology,* 2008, pp. 504-507.

[14] H. Eisele, "State of the art and future of electronic sources at terahertz frequencies," *Electronics Letters,* vol. 46, *(26),* pp. s8-s11, 2010.

[15] A. Maestrini and J. V. Siles, "Signal generation by diode frequency multiplication," in *Fundamentals of Terahertz Devices and Applications* 2021, Available: https://doi.org/10.1002/9781119460749.ch9. DOI: 10.1002/9781119460749.ch9.

[16] I. Mehdi *et al*, "THz Diode Technology: Status, Prospects, and Applications," *Proceedings of the IEEE,* vol. 105, *(6),* pp. 990-1007, 2017. . DOI: 10.1109/JPROC.2017.2650235.

[17] J. V. Siles *et al*, "A New Generation of Room-Temperature Frequency-Multiplied Sources With up to 10× Higher Output Power in the 160-GHz–1.6-THz Range," *IEEE Transactions on Terahertz Science and Technology,* vol. 8, *(6),* pp. 596-604, 2018. DOI: 10.1109/TTHZ.2018.2876620.

[18] T. J. Flack, B. N. Pushpakaran and S. B. Bayne, "GaN technology for power electronic applications: a review," *J Electron Mater,* vol. 45, *(6),* pp. 2673-2682, 2016.

[19] S. J. Pearton *et al*, "Fabrication and performance of GaN electronic devices," *Materials Science and Engineering: R: Reports,* vol. 30, *(3-6),* pp. 55-212, 2000.

[20] A. Hassan, Y. Savaria and M. Sawan, "GaN integration technology, an ideal candidate for high-temperature applications: A review," *IEEE Access,* vol. 6, pp. 78790-78802, 2018.

[21] F. Roccaforte and M. Leszczynski, *Nitride Semiconductor Technology: Power Electronics and Optoelectronic Devices.* John Wiley & Sons, 2020.

[22] H. Kroemer, "Theory of the Gunn effect," *Proceedings of the IEEE,* vol. 52, *(12),* pp. 1736, 1964.

[23] C. Sevik and C. Bulutay, "Gunn oscillations in GaN channels," *Semiconductor Science and Technology,* vol. 19, *(4),* pp. S188, 2004.

[24] R. F. Macpherson, G. M. Dunn and N. J. Pilgrim, "Simulation of gallium nitride Gunn diodes at various doping levels and temperatures for frequencies up to 300 GHz by Monte Carlo simulation, and incorporating the effects of thermal heating," *Semiconductor Science and Technology,* vol. 23, *(5),* pp. 055005, 2008.

[25] S. García *et al*, "Comparative Monte Carlo analysis of InP-and GaN-based Gunn diodes," *J. Appl. Phys.,* vol. 115, *(4),* pp. 044510, 2014.

[26] E. Alekseev and D. Pavlidis, "Large-signal microwave performance of GaN-based NDR diode oscillators," *Solid-State Electronics,* vol. 44, *(6),* pp. 941-947, 2000.

[27] S. García *et al*, "Numerical study of sub-millimeter Gunn oscillations in InP and GaN vertical diodes: Dependence on bias, doping, and length," *J. Appl. Phys.,* vol. 114, *(7),* pp. 074503, 2013.

[28] S. Garcia-Sanchez *et al*, "Optimization of the Epilayer Design for the Fabrication of Doped GaN Planar Gunn Diodes," *IEEE Trans. Electron Devices,* vol. 69, *(2),* pp. 514-520, 2021.

[29] O. Yilmazoglu *et al*, "Measured negative differential resistivity for GaN Gunn diodes on GaN substrate," *Electronics Letters,* vol. 43, *(8),* pp. 480-482, 2007.

[30] O. Yilmazoglu *et al*, "First Observation of Bias Oscillations in GaN Gunn Diodes on GaN Substrate," *Electron Devices, IEEE Transactions On,* vol. 55, *(6),* pp. 1563-1567, 2008.

[31] A. S. Hajo *et al*, "Reliable GaN-Based THz Gunn Diodes With Side-Contact and Field-Plate Technologies," *IEEE Access,* vol. 8, pp. 84116-84122, 2020. DOI: 10.1109/ACCESS.2020.2991309.

[32] A. M. Song *et al*, "Unidirectional electron flow in a nanometer-scale semiconductor channel: A self-switching device," *Appl. Phys. Lett.,* vol. 83, *(9),* pp. 1881-1883, 2003. Available: https://doi.org/10.1063/1.1606881. DOI: 10.1063/1.1606881.

[33] K. Y. Xu, G. Wang and A. M. Song, "Gunn oscillations in a self-switching nanodiode," *Appl. Phys. Lett.,* vol. 93, *(23),* pp. 233506, 2008. Available: https://doi.org/10.1063/1.3042268. DOI: 10.1063/1.3042268.

[34] J. Millithaler *et al*, "Optimized V-shape design of GaN nanodiodes for the generation of Gunn oscillations," *Appl. Phys. Lett.,* vol. 104, *(7),* pp. 073509, 2014.

[35] J. Mateos *et al*, "Design and fabrication of planar gunn nanodiodes based on doped GaN," in *2019 IEEE Asia-Pacific Microwave Conference (APMC),* 2019, pp. 971-973.

[36] S. Garcia-Sanchez *et al*, "Non-linear thermal resistance model for the simulation of high power GaN-based devices," *Semicond. Sci. Technol.,* vol. 36, *(5),* pp. 055002, 2021. . DOI: 10.1088/1361-6641/abeb83.

[37] M. Agrawal *et al*, "GaN-based SSD structure for THz applications," in *2019 IEEE Asia-Pacific Microwave Conference (APMC),* 2019, pp. 213-215.

[38] M. Piccardo *et al*, "Determination of the first satellite valley energy in the conduction band of wurtzite GaN by near-band-gap photoemission spectroscopy," *Physical Review B,* vol. 89, *(23),* pp. 235124, 2014.

[39] S. Wu *et al*, "Time-resolved intervalley transitions in GaN single crystals," *J. Appl. Phys.,* vol. 101, *(4),* pp. 043701, 2007. Available: https://doi.org/10.1063/1.2496399. DOI: 10.1063/1.2496399.

[40] S. Chen and G. Wang, "High-field properties of carrier transport in bulk wurtzite GaN: A Monte Carlo perspective," *J. Appl. Phys.,* vol. 103, *(2),* pp. 023703, 2008.

[41] Z. Zheng, Y. Mai and G. Wang, "Monte Carlo study of device characteristics of GaN-based avalanche photodiode devices," *J. Appl. Phys.,* vol. 106, *(2),* pp. 023716, 2009.

[42] S. García-Sánchez *et al*, "Non-linear thermal resistance model for the simulation of high power GaN-based devices," *Semiconductor Science and Technology,* vol. 36, *(5),* pp. 055002, 2021.

[43] F. Bertazzi, M. Moresco and E. Bellotti, "Theory of high field carrier transport and impact ionization in wurtzite GaN. Part I: A full band Monte Carlo model," *J. Appl. Phys.,* vol. 106, *(6),* pp. 063718, 2009.

[44] M. V. Fischetti, "Monte Carlo simulation of transport in technologically significant semiconductors of the diamond and zinc-blende structures. I. Homogeneous transport," *IEEE Trans. Electron Devices,* vol. 38, *(3),* pp. 634-649, 1991.

[45] B. G. Vasallo *et al*, "Monte Carlo study of kink effect in short-channel InAlAs/InGaAs high electron mobility transistors," *J. Appl. Phys.,* vol. 94, *(6),* pp. 4096-4101, 2003.

[46] L. Cao *et al*, "Experimental characterization of impact ionization coefficients for electrons and holes in GaN grown on bulk GaN substrates," *Appl. Phys. Lett.,* vol. 112, *(26),* pp. 262103, 2018. Available: https://doi.org/10.1063/1.5031785. DOI: 10.1063/1.5031785.

[47] D. Ji and S. Chowdhury, "On impact ionization and avalanche in gallium nitride," *Appl. Phys. Lett.,* vol. 117, *(25),* pp. 252107, 2020. Available: https://doi.org/10.1063/5.0031504. DOI: 10.1063/5.0031504.

[48] T. Maeda *et al*, "Impact ionization coefficients and critical electric field in GaN," *J. Appl. Phys.,* vol. 129, *(18),* pp. 185702, 2021. Available: https://doi.org/10.1063/5.0050793. DOI: 10.1063/5.0050793.

[49] I. Iñiguez-De-La-Torre *et al*, "Influence of the surface charge on the operation of ballistic T-branch junctions: a self-consistent model for Monte Carlo simulations," *Semiconductor Science and Technology,* vol. 22, *(6),* pp. 663, 2007.

[50] P. Sangaré *et al*, "Experimental demonstration of direct terahertz detection at room-temperature in AlGaN/GaN asymmetric nanochannels," *J. Appl. Phys.,* vol. 113, *(3),* pp. 034305, 2013. Available: https://doi.org/10.1063/1.4775406. DOI: 10.1063/1.4775406.

[51] J. M. Barker *et al*, "Bulk GaN and AlGaN/GaN heterostructure drift velocity measurements and comparison to theoretical models," *J. Appl. Phys.,* vol. 97, *(6),* pp. 063705, 2005. Available: https://doi.org/10.1063/1.1854724. DOI: 10.1063/1.1854724.